Comprehensive in-mould state monitoring of Material Jetting additively manufactured and machined aluminium injection moulds

Szabolcs Krizsma [a], András Suplicz [a,b,*]

[a] *Department of Polymer Engineering, Faculty of Mechanical Engineering, Budapest University of Technology and Economics, Műegyetem rkp. 3., H-1111 Budapest, Hungary*
[b] *MTA-BME Lendület Lightweight Polymer Composites Research Group, Műegyetem rkp. 3., H-1111 Budapest, Hungary*

ARTICLE INFO

ABSTRACT

The rapid evolution of additive manufacturing (AM) technologies is expected to revolutionize the injection moulding industry as well. AM technologies can be used to manufacture injection mould inserts. Several polymeric additive technologies like Material Jetting (including PolyJet), Material Extrusion (including Fused Deposition Modeling (FDM)) and Powder Bed Fusion (including Selective Laser Sintering (SLS)) can make mould inserts that are suitable for small series production. Metal inserts, made of steel or bronze can also be produced by Powder Bed Fusion (for example by Direct Metal Laser Sintering (DMLS)). These are comparable to their traditional, machined counterparts, regarding longevity and dimensional accuracy. In our study, we made inserts by Material Jetting (PolyJet) from an epoxy acrylate resin and compared its in-mould behaviour to a reference mould insert machined from aluminium. We measured the operational strains, cavity pressure and temperature distribution of the inserts. Operational strains exceeded 2 % in the case of the epoxy-acrylate insert. However, strains of the aluminium insert remained below 0.03 % for the aluminium insert under the same operational conditions. We set up correlational diagrams to numerically specify the load-deformation curve of the mould inserts. We also applied 3D scanning to measure the deformation of the inserts and injection moulded products alike. We found that scanning the injection moulded products yields more information about operational deformation of the inserts than scanning the inserts themselves.

1. Introduction

Additive technologies have already revolutionized both product and tool manufacturing. They can make moulds for conventional technologies like injection moulding. That is a fast evolving branch of Rapid Tooling (RT). Several promising results are already available on the applicability of RT moulds. Direct Metal Laser Sintering (DMLS) is capable of making middle to high-volume moulds quite accurately, reducing machining and finishing requirements. Optimized free-form lattice structures that improve the thermal cycling of hot stamping dies are manufacturable by DMLS printing [1]. Injection mould inserts with conformal cooling channels can also be produced by DMLS and additional machining delivers excellent dimensional accuracy. Furthermore, surface treatment can adjust the surface hardness and strength of the moulds [2]. Additively manufactured maraging steel injection mould inserts with conformal cooling channels reduce cycle

time significantly and greatly improve the surface quality of polymer products [3,4]. Numerical simulations help design geometrically complex, optimized conformal cooling channel layouts that can be produced by a combination of DMLS and CNC machining. These inserts can achieve significant cycle time reduction compared to conventionally cooled, machined inserts [5,6]. The corrosion resistance and strength of martensitic maraging stainless steel printed by Laser Powder Bed Fusion (LPBF) can be enhanced—this way, complex, high-volume injection moulds can be produced [7]. DMLS–printed metallic injection mould inserts have already reached several thousand cycles without observable tool wear [8]. Other research concluded that a combination of polymer coated metal 3D printing (indirect SLS) and additional machining is competitive with conventional mould making [9]. Filaments made of polymer coated metal powder are also suitable for mould making [10].

Alongside metal moulds produced by additive technologies, 3D printed polymeric moulds are also gaining ground in low-volume

---

production. Thermoplastic technologies, FDM and SLS are both suitable to make parts and prototype moulds as well [11–15]. FDM is an especially popular AM technology because of its low cost and widespread application. Researchers already analyse the mechanical properties of FDM printed thermoplastic specimens and parts [16–19]. Residual stresses in FDM printed parts and the resulting product warpage is also in the focus of the research community [20,21]. Researchers also analyse the feasibility of FDM printing aluminium alloys [22]. Despite the research interest, publications discussing the applicability of FDM printing to produce conventional injection moulds are rare to find. However, several comparative studies of thermoplastic polymer printing technologies are available. A key requirement for injection moulds is always dimensional accuracy. A comparative study of FDM, SLS and Arburg Freeformer printed parts concluded that minimal layer thickness has a significant effect on part accuracy. Another finding was that accuracy of powder-based technologies like SLS depend heavily on adhesion between particles [23]. Conformally cooled mould inserts for wax injection moulding can also be printed by FDM, among others, from an aluminium-filled filament [24]. FDM printing can make thermoplastic patterns for investment casting that can be proper replacements of traditional wax patterns [25]. FDM printed moulds are also applicable for vacuum assisted resin transfer moulding (VARTM) because mould dimensions tend to stabilise after a small number of thermal cycles [26].

The other main group of polymeric additive technologies uses non-thermoplastic materials, typically epoxy-acrylic resins. In our previous study, we produced a complex state monitoring system of epoxy acrylate inserts to measure the operational strain, cavity pressure and temperature of PolyJet printed inserts [27]. PolyJet printing also allows widely variable conformal cooling channel layouts. Optimal conformal cooling channels and a careful choice of mould material can reduce mould insert surface temperature below the glass transition temperature, which is vital to the long life of prototype moulds [28]. The surface temperature distribution of epoxy acrylate injection moulds can be predicted with adequate accuracy by injection moulding simulation [29]. In-depth failure analysis of inserts made by vat photo-polymerization is already available. Finite element simulations can calculate temperature distribution and induced stresses in the part and can show insert failure locations during injection moulding [30].

Some research is also available on the comparison of thermoplastic and non-thermoplastic additively manufactured moulds and patterns [31]. Wang et al. [32] manufactured wax patterns for investment casting by SLS from HIPS and by SLA from a photopolymer resin. They found thermoplastic HIPS patterns effective for investment casting. Wick-Joliat et al. [33] created prototype moulds for ceramic injection moulding (CIM) by FDM from PVA and by digital light processing (DLP) from a water-soluble resin. They managed to injection mould complex three-dimensional coil-shaped products using the prototype moulds and found that DLP printed moulds have higher resolution than their FDM printed counterparts.

Mould material and the resulting cooling speed also has a profound effect on the crystallinity and mechanical properties of the injection moulded part. Polypropylene parts injection moulded into a PolyJet printed DigitalABS mould show significantly different crystallinity compared to parts injection moulded into a machined aluminium mould. Therefore, tensile specimens injection moulded with the DigitalABS mould showed lower strain at break and lower strain at yield, while a higher Young's modulus and stress at yield [34]. Tábi et al. [35] had similar findings when they injection moulded PLA into a DigitalABS mould and into a conventional steel mould. They also found that nucleated PLA processed with a low thermal conductivity DigitalABS mould showed significantly higher crystallinity compared to PLA injection moulded into a steel mould. DigitalABS is a popular choice for rapid injection mould making [36].

New prototype mould–making techniques allow injection moulders to check their designs in a real operational environment before costly and time-consuming conventional mould machining. New and complex geometries can be manufactured, like conformal cooling channels, which are vital for decreasing cycle time and increasing productivity. Prototype moulds might bring design flaws to surface early in the mould making process, resulting in the much desired reduction of cost and development time. Because of these potential benefits of RT moulds, their practical application is expected to become widespread in the near future. Although several case studies are available on the application of different RT moulds, experts have not used comprehensive state monitoring to numerically characterize their operational behaviour until now. The aim of our research is to quantify the operational strain, cavity pressure and temperature distributions of an additively manufactured epoxy acrylate insert and a conventional machined aluminium insert. With this comprehensive state monitoring, we can highlight the main differences in their in-mould behaviour and help adjust injection moulding parameters to reach the maximum possible lifetime of polymeric moulds. This type of process parameter quantification and numeric comparison of the different mould making techniques is new and it adds to the already existing state of the art.

2. Materials and methods

2.1. The mould and the mould inserts

We used additively manufactured mould inserts which were printed by PolyJet. This is a commercially available technology based on the principle of material jetting. The printer head containing the piezo-electric nozzles injects small resin droplets and support material in the building space, then a robust UV lamp cures the resin. The support material is typically water-soluble so it can be easily removed after printing. The layer thickness of the printing was 28 μm, the build time was 3 h and 43 min and the build orientation is indicated in Fig. 1. As reference, we chose a machined aluminium insert. The overall dimensions of the inserts were 75 mm × 65 mm × 15 mm. The injection moulded product was a plate with overall dimensions of 65 mm × 55 mm × 2 mm. Additionally, four cylindrical slots (15 mm diameter and 7 mm depth each) were placed at the back of the inserts for strain measurement and two of them were fitted with strain gauges (*KMT-LIAS-06-3-350-5EL*). The signals of the strain gauges were collected by a *Spider 8* unit. We also placed a thermocouple (*Heraeus M222, Pt100*) for temperature measurement at the back of the insert in a racetrack-shaped groove (18 mm × 5 mm × 3 mm). Both strain gauges and the thermocouple were fixed with a cyanoacrylate adhesive (*3 M Scotch Weld Plastic and Rubber Instant Adhesive PR100*). The moving side mould insert with the strain gauges and the thermocouple can be seen in Fig. 1.

We measured cavity pressure directly with an *RJG 6159 Piezo* pressure sensor and its data was gathered by a *Kistler Como Injection 2869B* data collector. The pressure sensor was built into the fixed side mould insert with a retaining sleeve. The pressure sensor was mounted with an offset from the centre of the cavity, therefore pressure can be measured both at the near gate and the far from the gate locations if the mould inserts are rotated by 180°.

We assembled the inserts into a two-cavity steel mould housing. The moving half, with the ejection system and the fixed side of the mould can be seen in Fig. 2 a) and b), respectively. As can be seen, the cavity was filled through an edge gate.

2.2. Materials

The reference insert was machined from the *EN AW 5754 O/H111* aluminium alloy. Relevant mechanical and thermal properties of the material are listed in Table 1. The AM mould inserts were made by PolyJet, with an *Objet Alaris 30, (Stratasys Ltd.)* printer. The inserts were made from an UV-curable epoxy acrylate resin, *VeroWhite Plus* (also known as *RGD 835*) manufactured by *Stratasys Ltd*. Important mechanical and thermal properties of the material are listed in Table 1.

The injection moulded material was a homo-polypropylene; its
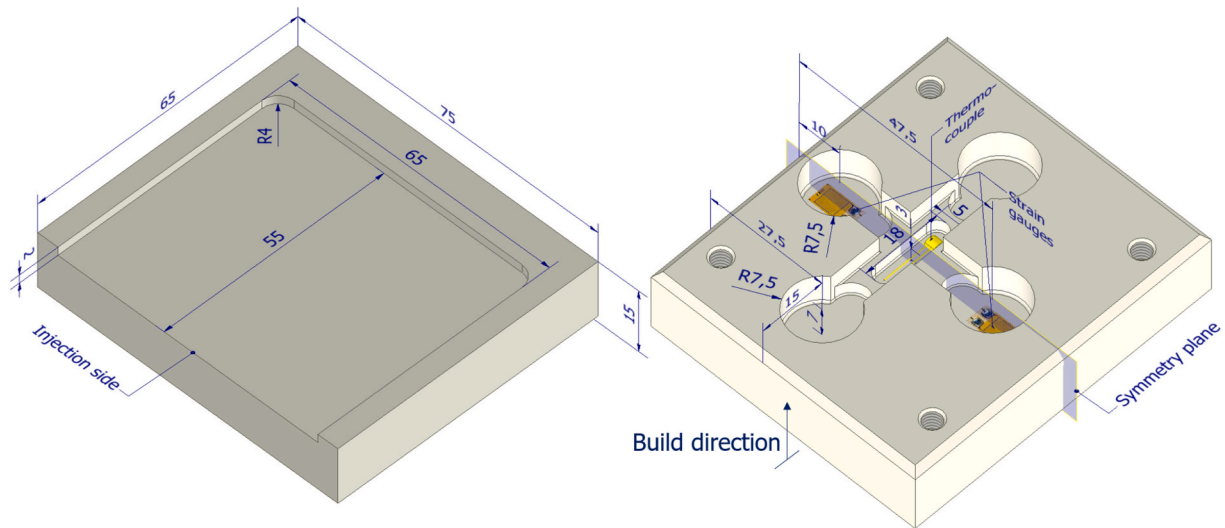
Fig. 1. The moving side mould insert, the positions of the strain gauges and the thermocouple. (All the dimensions are in mm.)
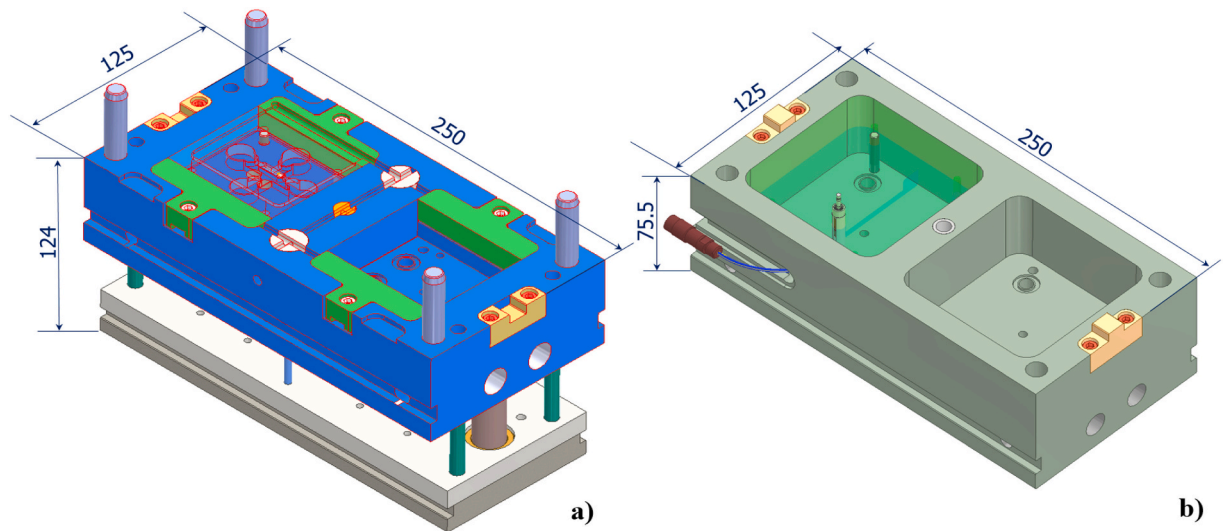
Fig. 2. The moving half of the mould with the ejection system a) and the fixed half of the mould b).

Table 1
The physical properties of *EN AW 5754* and *Stratasys RGD835*.

Physical properties	Unit	EN AW 5754 O/H11	VeroWhite (RGD835)
Tensile strength	MPa	160–200	50–65
Elongation at break	%	12	10–25
Modulus of elasticity	GPa	68	2–3
Flexural strength	MPa	–	75–110
Flexural modulus	GPa	–	2.2–3.2
Maximal service temperature	°C	160	45–50 (HDT) (0.45 MPa)
Glass transition temperature	°C	–	52–54
Thermal conductivity	W/(m·K)	147	0.2
Coefficient of thermal expansion	1/K	$24 \cdot 10^{-6}$	$\sim 75 \cdot 10^{-6}$

Table 2
The typical physical properties of *Tipplen H145F*.

Physical properties	Unit	Typical value
Melt flow rate (MFR) (230 °C/2.16 kg)	g/10 min	29
Flexural modulus	GPa	1.8
Module of elasticity (in tension)	GPa	1.99
Tensile stress at yield	MPa	38
Tensile strain at yield	%	8
Recommended processing temperature	°C	190–235

3. Comprehensive state monitoring of additively manufactured mould inserts

To compare the in-mould behaviour of different inserts, we devised a comprehensive state monitoring method. In addition to strain, temperature and cavity pressure measurement, the surface temperature distribution of the inserts after mould opening was also measured, with a *FLIR A325sc* thermal imaging camera. Fig. 3 shows a graphical interpretation of the comprehensive state monitoring method.

commercial name is *Tipplen H145 F*. It was purchased from *MOL Group Public Limited Company*. Important material properties can be found in Table 2.
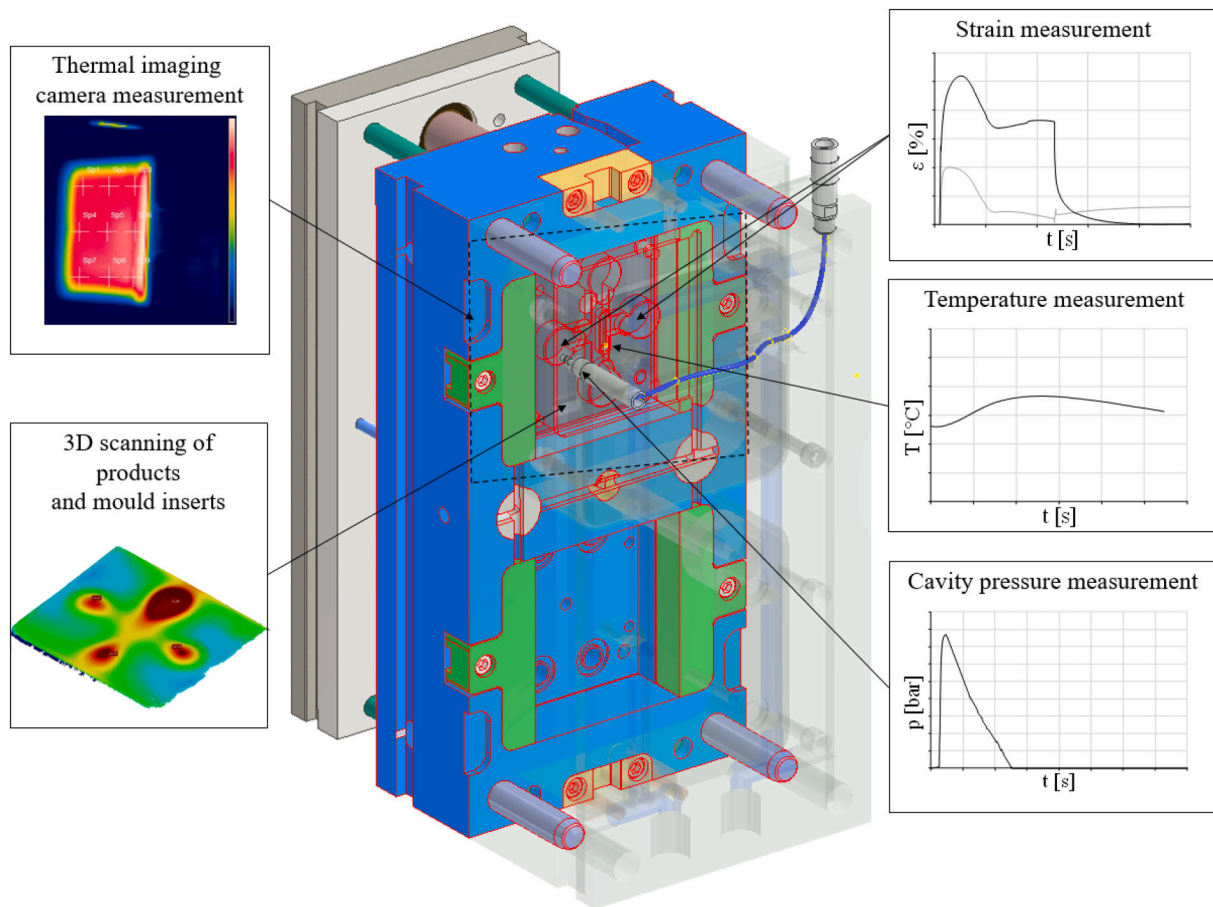
Fig. 3. Schematics of the comprehensive state monitoring of mould inserts.

3.1. Filling tests and injection moulding parameters

We injection moulded using an *Arburg Allrounder Advance 270S 400-170* injection moulding machine (*ARBURG GmbH*) with a screw diameter of 30 mm. Injection speed was 15 cm³/s, clamp force was 5 tons, injection pressure limit was 500 bars, holding time was 15 s, residual cooling time was 30 s and dose volume was 40 cm³. To allow the epoxy acrylate insert to cool below its T_g, we left approximately 300 s idle time between the cycles. To find the proper switchover point, first we carried out a mould filling test. We started injection moulding at a switchover point of 35 cm³ and decreased it in 2 cm³ steps to reach complete volumetric filling. We found the optimal switchover point at 26 cm³ (in the 6th cycle). The filling pattern for the aluminium insert can be seen in Fig. 4.

We carried out thermal imaging camera measurements in the idle time between the cycles, in the open state of the mould. An important observation during the filling test of the epoxy acrylate insert was that the low thermal conductivity of the material resulted in a high-temperature zone concentrated approximately around the contour of

the short-shot products. These results are shown in Fig. 5. Gradual, cycle-to-cycle heating of the cavity is best shown in the vicinity of the edge gate, as high temperature zones (indicated in red) originate from the edge gate and follow the filling pattern of the cavity.

After finding the switchover point corresponding to complete volumetric filling, we analysed the effect of cyclic loading at a constant holding pressure. We injection moulded 10 cycles with a holding pressure of 75 bar to measure in-mould behaviour of inserts at constant injection moulding parameters. After that, we increased holding pressure starting from 50 bar using 25 bar increments in every second cycle.

3.2. In-mould behaviour of epoxy acrylate inserts with constant injection moulding parameters

In the first section of our main experiments with the epoxy acrylate inserts, we injection moulded with a constant holding pressure (75 bar). We measured strain at two locations: near and far from the edge gate. The measured strain curves are presented in Fig. 6.

It can be seen that in the 1st cycle, the gauges near and far from the
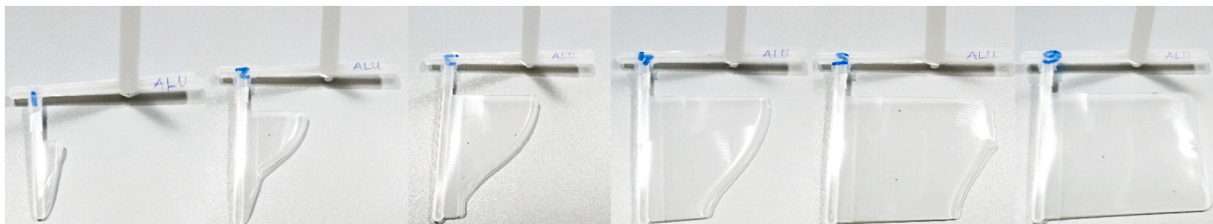
Fig. 4. Mould filling pattern for the aluminium insert.
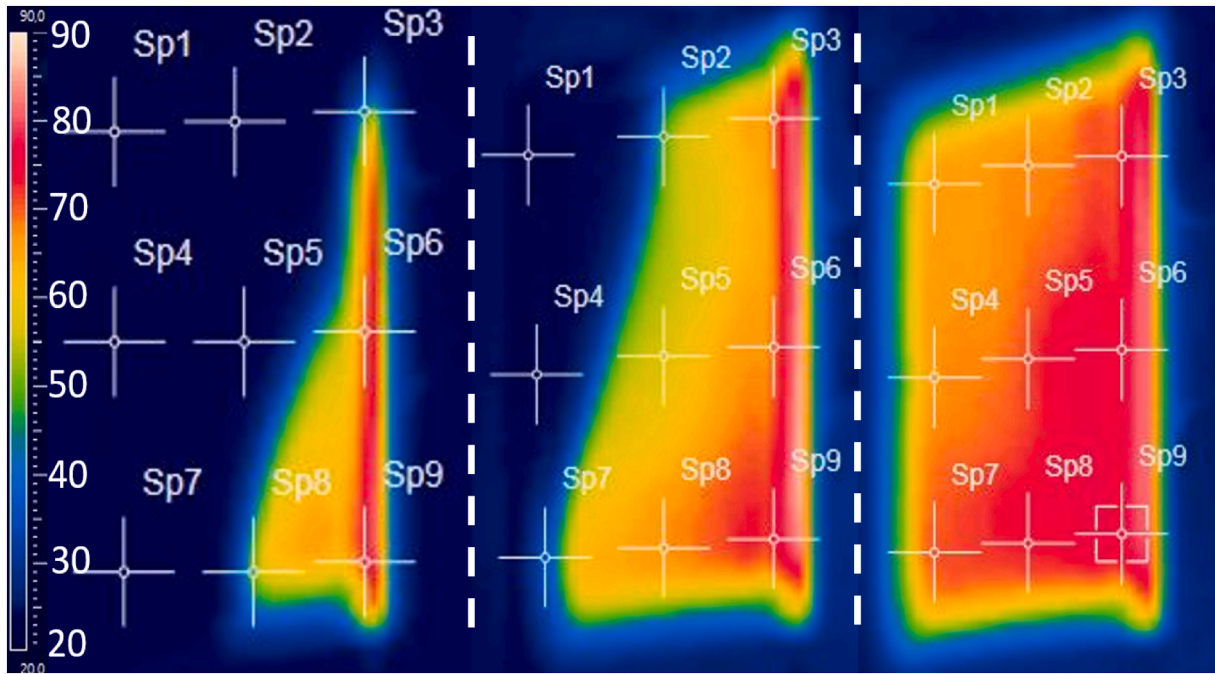
Fig. 5. Thermal imaging camera results of the epoxy acrylate insert filling test (2nd, 4th and 6th cycles).
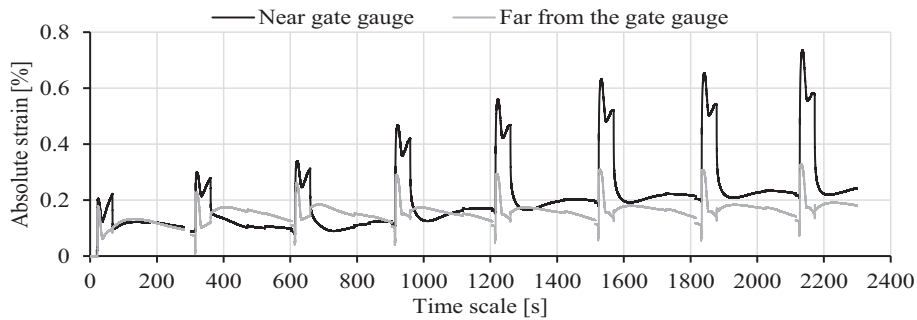
Fig. 6. Strain measurement results of the gauges near and far from the gate and with a constant holding pressure of 75 bar.

gate measured very similar maximal absolute strain. However, as we injection moulded more cycles, the accumulation of strain became more dominant at the near gate location as it was subjected to higher cavity pressure and thermal load. The effect of soft tool material is evident, as not even 300 s of constant cycle time allowed the strain of the insert to decrease substantially. Table 3 shows maximal absolute strains in each cycle, residual strains at the end of the delay time and maximal cavity

Table 3
Strain and cavity pressure results of the epoxy acrylate insert.

Cycle number	Maximal absolute strain near the gate	Maximal absolute strain far from the gate	Residual strain near the gate	Residual strain far from the gate	Maximal cavity pressure
[−]	[%]	[%]	[%]	[%]	[bar]
1	0.22*	0.18	0.10	0.09	N/A
2	0.30	0.23	0.10	0.13	N/A
3	0.34	0.26	0.12	0.12	67.6
4	0.47	0.29	0.17	0.12	71.7
5	0.56	0.29	0.20	0.13	76.0
6	0.63	0.31	0.21	0.14	80.0
7	0.65	0.31	0.22	0.14	78.9
8	0.74	0.33	0.24	0.18	76.9

* measured at part ejection.

pressure. In 8 cycles with constant holding pressure, maximal absolute strain more than tripled at the near gate location (from 0.22 % to 0.74 %) and it almost doubled at the location far from the gate (from 0.18 % to 0.33 %). The tendency is similar for residual strains. Gradual deformation of mould inserts also resulted in a slight change in maximal cavity pressure, but the uncertainty of switchover in the case of a hydraulic injection moulding machine also influences maximal cavity pressure.

As can be seen from Table 3, residual strain gradually increased in each cycle at the locations both near and far from the gate. As a result, absolute strain characterizes cumulative deformation. In order to numerically specify strain change within a single cycle, we introduced relative strain, that is, the difference of absolute strain in the actual cycle and residual strain from the previous cycle (1):

$$\varepsilon_{rel,i}(t) = \varepsilon_{abs,i}(t) - \varepsilon_{res,i-1} \qquad (1)$$

where $\varepsilon_{rel,i}(t)$ is the relative strain in the ith cycle, $\varepsilon_{abs,i}(t)$ is the absolute strain in the ith cycle and $\varepsilon_{res,i-1}$ is the residual strain from the $(i-1)^{th}$ cycle.

The introduction of relative strain helps to characterize the speed at which deformation accumulates. If relative strain remains constant from cycle to cycle, it means that the deformation of the insert at the analysed point stabilised and the accumulation of strain is less significant. On the

other hand, if relative strain increases in every cycle, it means a progressive growth in deformation at the analysed point. Fig. 7 a) and b) present relative strains near and far from the gate, respectively. As can be seen, the near gate location shows a clearly progressive growth in maximal relative strain, starting from 0.21 % in the 2nd cycle to 0.52 % in the 8th cycle. On the other hand, relative strain curves stabilise at the location far from the gate and a relative strain maximum of approximately 0.2 % can be observed in each cycle.

It is also worth noting that the main segments of the injection moulding cycle can be clearly observed in the relative strain–time curves. The first, steep segment is the filling phase (fill time ~ 1.2 s) where the elastic deformation component is dominant. This is followed by the holding phase (15 s) where a relative strain maximum occurs, prolonged in time. In the holding phase, all three deformation components of the polymeric mould insert (elastic, viscoelastic and viscous) occurs. Maximal relative strains are significantly higher near the gate than far from the gate that is caused by two factors. The first cause is that the pressure of the melt drops along the flow length and the second is that the local heat transfer from the melt to the mould insert is also dependent on the pressure. As holding pressure is dropped, residual cooling time begins, where the cooling product shrinks, thus giving free space to the cavity to spring back, resulting in a decrease in relative strain. On the other hand, slow heat transfer from the injected polymer melt in the residual cooling time increases insert temperature, which causes thermal expansion and a slight increase in strain. It also has to be considered that the stiffness of polymeric mould inserts is also heavily dependent on temperature. Loss of stiffness due to heat also results in increased strain. Thermal expansion and loss of stiffness happens later than the starting point of the injection moulding cycle. Heating of the insert is slow due to two reasons: first, the thermal conductivity of epoxy acrylate is low (~ 0.2–0.3 W/(m·K)) [37], while its specific heat is high (1000–2000 J/(kg·K)) [37], and second, the heat transfer coefficients between the melt and the cavity wall are also modest, due to the much lower applicable holding pressure compared to metal mould inserts. At mould opening and part ejection, there is a steep decrease in strain as the elastic deformation component still remaining in the insert instantaneously disappears. On the near gate strain curves, part ejection is marked by a sharp decrease, while on the curves measured far from the gate, a minor increase can be observed. It is caused by the ejector pins, which are located in the runner—they slightly bend the part towards the location far from the gate upon ejection.

It is worth comparing the relative strain and cavity pressure results of the epoxy acrylate insert with the aluminium insert when the injection moulding parameters are the same (75 bar holding pressure). These results are shown in Fig. 8 a) for the epoxy acrylate insert and b) for the aluminium insert. The first significant difference is in the magnitude of relative strain. In the case of the epoxy acrylate insert, maximal relative strain in the 5th cycle is 0.40 %, compared to the 0.017 % of the aluminium insert which is a 23.5 time difference. This is in line with preliminary expectations, since the ratio of the two materials' elastic moduli at room temperature is in this range. The shape of the strain

curves is also different. In the case of the aluminium insert, no plateau can be seen in residual cooling time. Instead, after the maximum point, there is a steady decrease that also contains a sharp drop at mould opening and part ejection. The first significant difference in the cavity pressure curves is the maximum value: 76 bar for the epoxy acrylate insert and 18.2 bar for the aluminium insert. A possible cause of this difference is the thermal expansion of the inserts. The coefficient of thermal expansion of the epoxy acrylate insert is one magnitude higher than that of the aluminium insert. Since the polymer mould insert cannot expand into the direction of the steel mould housing, which has a modulus of elasticity approximately two magnitudes higher, it inevitably deforms towards the cavity. Therefore, cavity volume is lower in the case of the polymer mould insert, so the same injected melt volume necessarily results in higher cavity pressure. Lower cavity volume can be observed on the injection moulded products as well. Plates produced with the epoxy acrylate insert generally have lower thickness (starting from approximately 1.7 mm at a holding pressure of 50 bar). Product thickness and holding pressure shows a strong positive correlation. In the case of the aluminium insert, the thickness variation of the plates is not that significant (between 1.94 mm and 2 mm), as long as the clamping force is enough to prevent unwanted mould opening.

We also compared the thermal state of the epoxy acrylate and aluminium mould inserts. Surface temperatures (measured with a thermal imaging camera in the delay time between the cycles) and the temperature at the back side of the insert (measured with a thermocouple) are shown in Fig. 9.

Aluminium has a thermal conductivity two orders of magnitude higher than epoxy acrylate, this difference clearly shows in thermal imaging camera images. At the moment of mould opening, the surface temperature of the epoxy acrylate insert varies between 73 and 78 °C. On the other hand, the surface of the aluminium insert has already cooled down to 26 °C, which is nearly ambient temperature. At the end of the thermal imaging camera measurement, the surface temperature of the cavity of the epoxy acrylate insert varies between 41 and 48 °C, still well above ambient temperature. Thermocouple measurements also indicate a significant difference in thermal conductivity and specific heat. The maximum of the temperature of the back side of the epoxy acrylate insert is only reached in the delay time after mould opening (48 °C at 130 s from the beginning of the cycle). The temperature balance between cavity and the back side is reached at approximately 180 s when the curve of the thermocouple signal gradually intersects with thermal imaging camera measurement curves. The back side of the epoxy acrylate insert cools slightly more slowly than the cavity surface, indicated by the slope of the corresponding curves. On the other hand, the temperature of the back side of the aluminium insert increases fast and reaches its maximum of 32.6 °C well before mould opening. This is a clear consequence of the fast cooling of the product and rapid heat extraction.
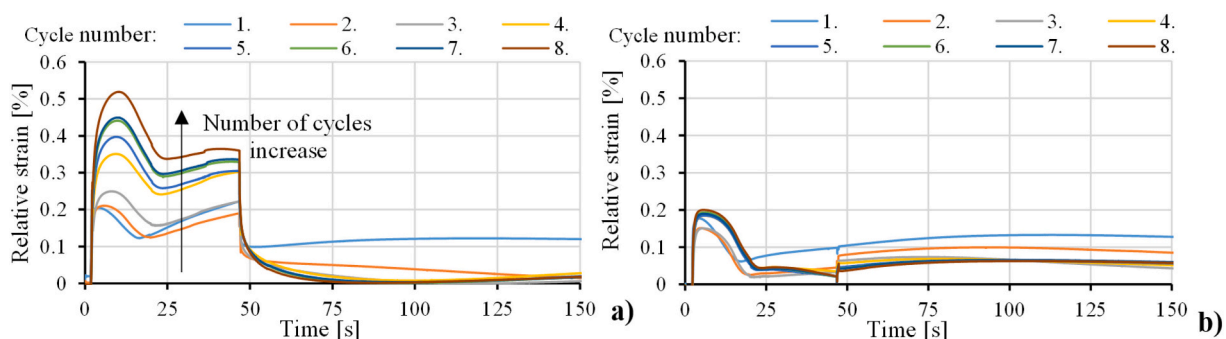
Fig. 7. Relative strain curves of the gauges near and far from the gate with a constant holding pressure of 75 bar.
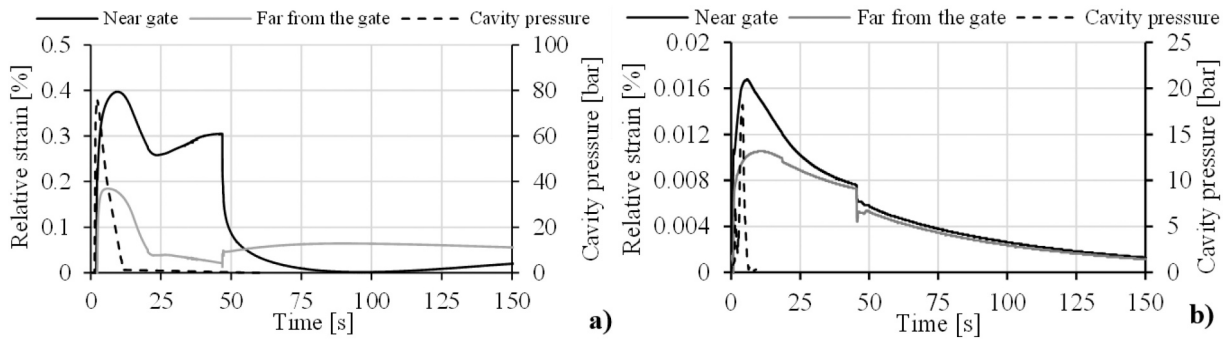
Fig. 8. Relative strain–time and cavity pressure–time curves with a holding pressure of a constant 75 bar for the epoxy acrylate insert (5th cycle) a) and the aluminium insert (filling–early holding phase) b).
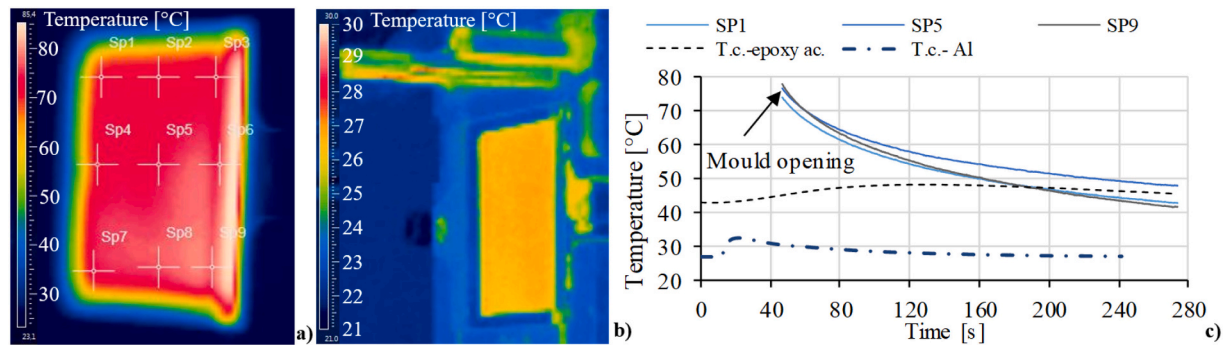
Fig. 9. Surface temperature distribution of the epoxy acrylate insert with a holding pressure of 75 bar (7th cycle) at mould opening a) aluminium insert with a holding pressure of 75 bar at mould opening b) and cooling curves of points in a) with the thermocouple results at the back side of the two inserts c).

3.3. In-mould behaviour of epoxy acrylate inserts with increasing holding pressure

After injection moulding ten cycles with constant holding pressure, we analysed the effect of increasing holding pressure. We started with a holding pressure of 50 bar and increased it in steps of 25 bar in every second cycle. The effect of increasing holding pressure on the relative strain–time curves of the epoxy acrylate insert is indicated in Fig. 10. It is clear that as we applied higher holding pressures, the maximum of relative strain (measured in the holding phase) increased as well. At higher holding pressures, relative strain stabilised at higher levels, later even increased further in residual cooling time and exceeded the maximum of the filling–holding phases. Higher holding pressure results

in more dominant creep both in the holding phase and in the residual cooling time. From the magnitude of relative strains, it is clear that deformation is more dominant at the location near the gate than at the location far from the gate. From the 21st cycle, a gradual failure of the near gate gauge is shown as ever longer discontinuities appear in its signal around the maximum points of the relative strain curves. In the 24th cycle, the near gate gauge provided no meaningful signal, indicating its permanent failure.

Relative strain–time curves are presented for the aluminium insert in Fig. 11. The first major difference between the epoxy acrylate and aluminium inserts is the magnitude of relative strains. In the case of the aluminium insert, maximal relative strain did not reach 0.03 %, which is in sharp contrast with the results of the epoxy acrylate insert. The other
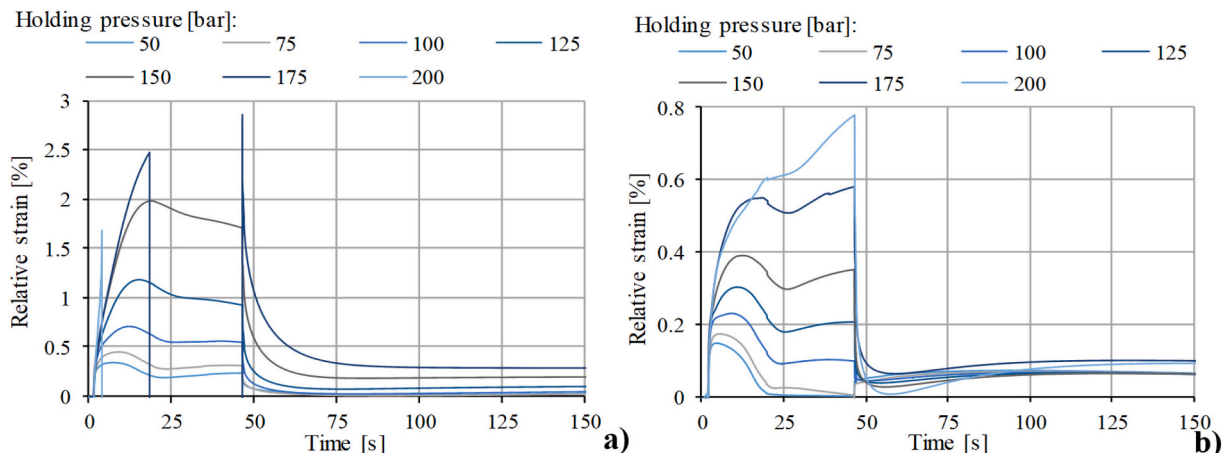
Fig. 10. Relative strain–time curves of the gauges near the gate a) and far from the gate b) with increasing holding pressure.
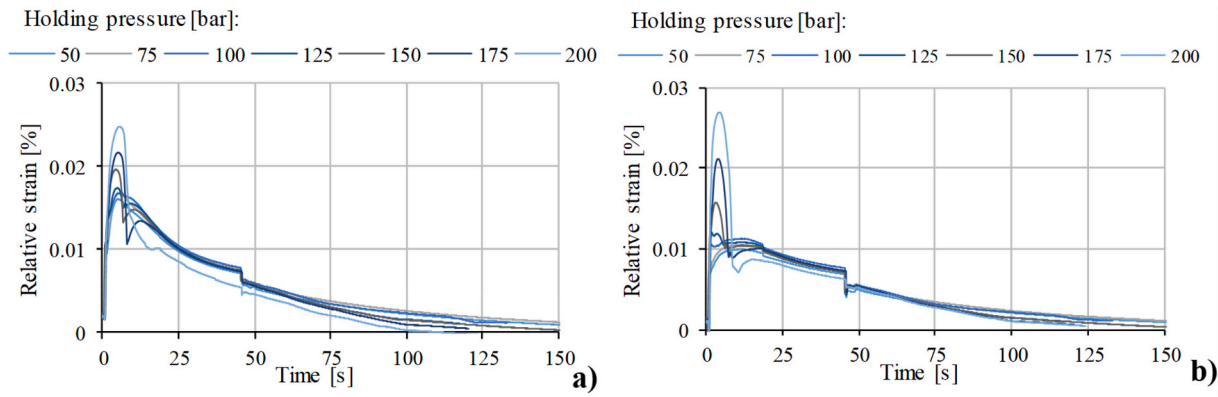
Fig. 11. Relative strain–time curves measured by the gauges near the gate a) and far from the gate b) with increasing holding pressure.

main difference is in the shape of the curves. In the case of the aluminium insert, maximum relative strain is almost instantaneously reached at the end of filling or early in the holding phase. As we applied higher holding pressures (150 to 200 bar), maximal relative strain became peaked (higher in magnitude but shorter in time) compared to lower holding pressures. After the maximum points, relative strain decreased steadily in residual cooling time and the delay time between the cycles. A small, step-like decrease can be observed on the relative strain–time curves, which corresponds with mould opening and part ejection. It is also important to note that the relative strains near the gate and far from the gate in the case of the aluminium insert are quite similar both in magnitude and shape. Therefore, the measurement location did not have such a profound effect on the results compared to the epoxy acrylate insert, where significant differences in strain can be observed between the two locations.

In the case of the epoxy acrylate insert, it is worth comparing relative strain and cavity pressure curves at two, significantly different holding pressures. Fig. 12 a) and b) show these results at 50 bar and 125 bar, respectively. Relative strains increased significantly at the locations both near the gate and far from the gate and the indicated delay in time between cavity pressure maximum and relative strain maximum also became longer. As holding pressure increased, so did cavity pressure and its decay became slower. At a holding pressure of 50 bar, cavity pressure dropped to zero at around 10 s, while at 125 bar it only reached zero at 20 s. The steep downturn at the end of the near-gate relative strain curve with a holding pressure of 125 bar indicates a large elastic deformation component, which almost instantaneously disappeared as the mould opened and the part was ejected. This can be the result of the more dominant creep of the epoxy acrylate insert and the increased product size, which further deformed the insert at a higher holding pressure.

After the 23rd cycle, the near-gate strain gauge ruptured and in the 24th cycle it did not provide any results. Therefore, we terminated the

measurement and disassembled the moving mould half. We scanned the injection moulded products of the 21st and 24th cycles and the moving side mould insert as well, using a *GOM ATOS Core* 3D scanner. These results are presented in Fig. 13. We found significant thickness variation above the 4 slots of the strain gauges (these were shown in Fig. 1). In the 21st cycle, product thickness at the near gate slot deviated by 0.9 mm from the nominal 2 mm and that difference further increased to 1.81 mm in the 24th cycle. There were also local shape changes above the other three slots but their scale was lower compared to the near gate location. These dimension changes are in line with preliminary expectations, since the near gate location is subjected to a high pressure and temperature load. Scanning the mould insert did not show significant residual deformation, so the mould insert had almost regained its original shape by the time of scanning. From these, the conclusion can be drawn that scanning the injection moulded products yields more information about operational deformation of the insert than scanning the insert itself.

3.4. Failure of the epoxy acrylate insert and product size deviation

After 3D scanning the epoxy acrylate mould insert, we reassembled the moving mould half and continued injection moulding. We injection moulded 10 cycles with a holding pressure of 125 bar, then 14 cycles with 175 bar and finally 6 cycles with 225 bar, until the insert failed. We were only able to measure strains at the location far from the gate because the near gate gauge had ruptured. Relative strain results for the gauge far from the gate are presented in Fig. 14. In the 10 cycles injection moulded with a holding pressure of 125 bar, relative strain decreased and then stabilised as shown in Fig. 14 a). After that, we increased holding pressure to 175 bar, which resulted in higher relative strains in the holding and residual cooling phases, compared to when holding pressure was 125 bar. Still, relative strain gradually decreased
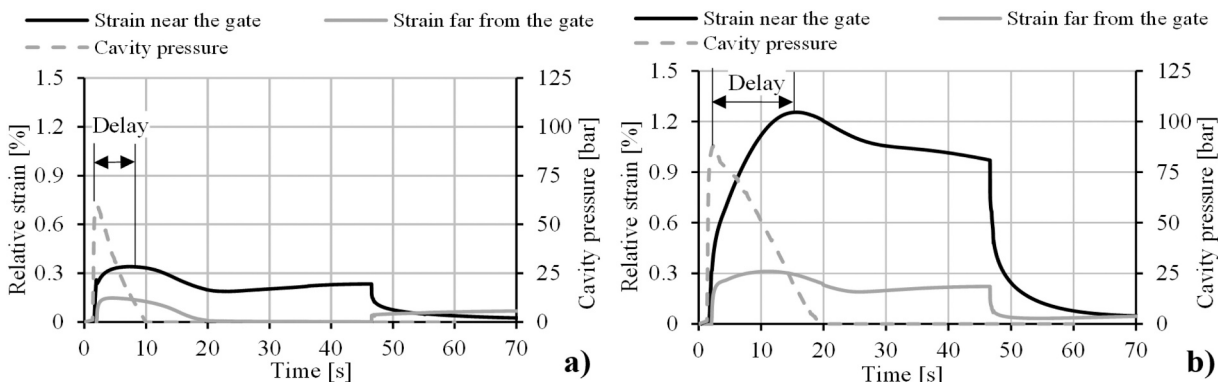
Fig. 12. Relative strain–time and cavity pressure–time curves of the epoxy acrylate insert when holding pressure is 50 bar a) and 125 bar b).
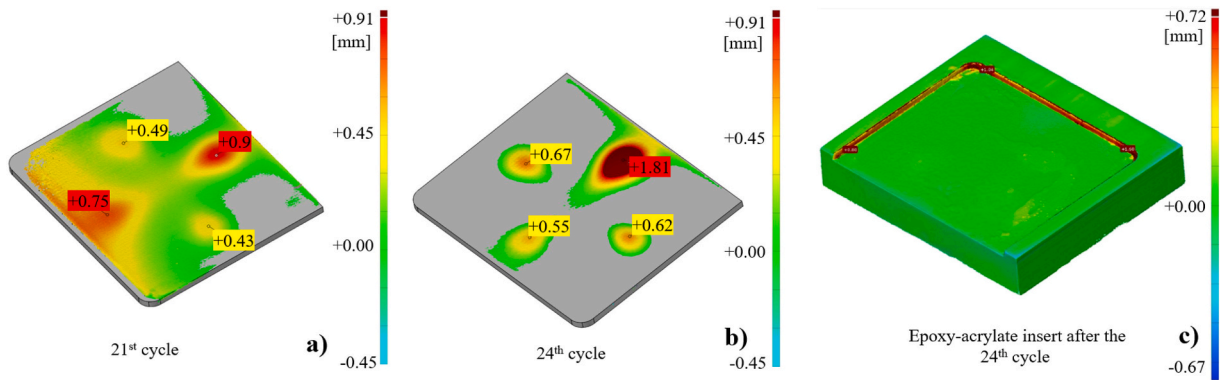
Fig. 13. 3D scanning images of the injection moulded product in the 21st cycle a), 24th cycle b) and the epoxy acrylate mould insert after the 24th cycle c).
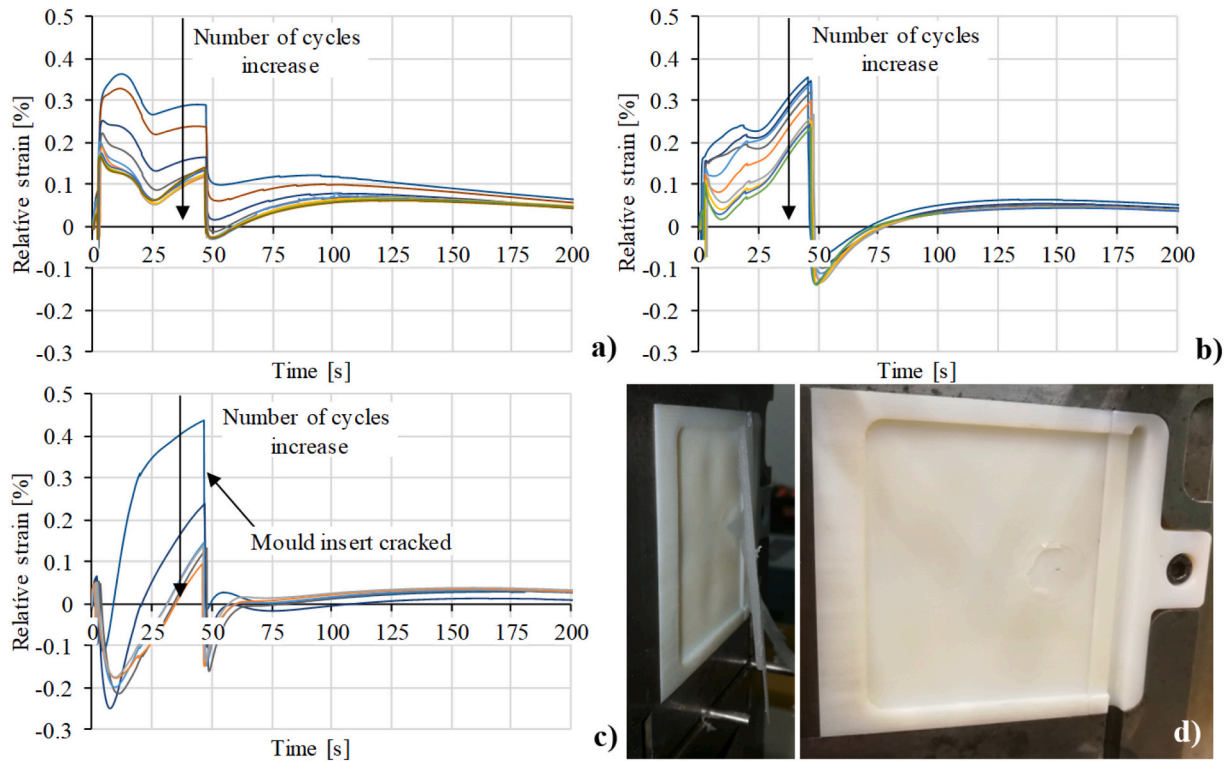
Fig. 14. Relative strain–time curves of the epoxy acrylate insert when holding pressure was a constant 125 bar a) when holding pressure was a constant 175 bar b) from crack initiation when holding pressure was a constant 175 bar c) and deformations with the failure location of the insert d).

from cycle to cycle under constant holding pressure. These results are presented in Fig. 14 b). This can be caused by the hardening of the insert material due to the repeated pressure and thermal load. The exact nature of hardening has to be subject of further investigation. The mould insert began to fracture in the 10th cycle when holding pressure was 175 bar. The fracture was clearly indicated in the corresponding relative strain–time curve because its shape changed drastically compared to the previous curves. After that cycle, maximal relative strain dropped sharply, as shown in Fig. 14 c). By this time, the insert was gradually perforated above the near gate slot. The strain gauge signal was lost completely in the last cycle when holding pressure was 175 bar. After that, we managed to injection mould another 6 cycles with a holding pressure of 225 bar until the melt completely punctured the cavity surface above the near gate slot. From these cycles, no strain measurement data could be gathered. In the last few cycles, the cavity surface of the insert deformed evidently above the slots of the strain gauges, as shown in the photos taken during the injection moulding series,

presented in Fig. 14 d).

Following the complete failure of the insert, we stopped injection moulding and disassembled the moving mould half to 3D scan the cracked insert. We scanned both the cavity side and the back side (Fig. 15). The punctured hole on the cavity surface is clearly shown and a larger part also broke out of the insert at the back side. Despite the clearly visible deformation of the cavity during injection moulding indicated in Fig. 14 d), no significant residual deformations can be observed on the scanned image of the cavity in Fig. 15. We found a similar phenomenon while first scanning the moving side mould insert (discussed in-detail in Fig. 13) The positive size deviation (indicated in red) inside the slot at the back side are the remnants of the thermocouple.

Increasing deformations during injection moulding cycles can be best observed on the injection moulded products. These results are presented in Fig. 16. Near gate deformation increased almost tenfold from 0.81 mm in the 8th cycle to 8.07 mm in the 37th cycle. Deformation also
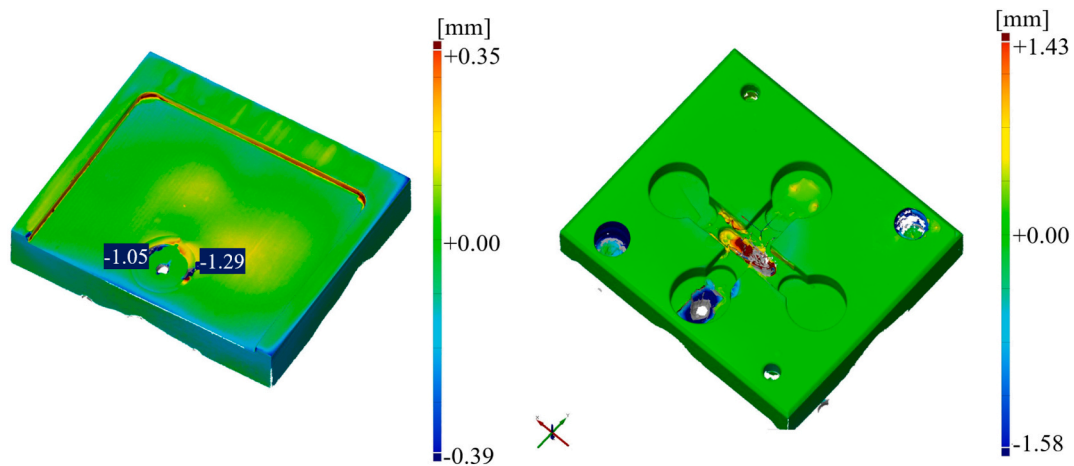
Fig. 15. 3D scanned image of the mould insert after failure.
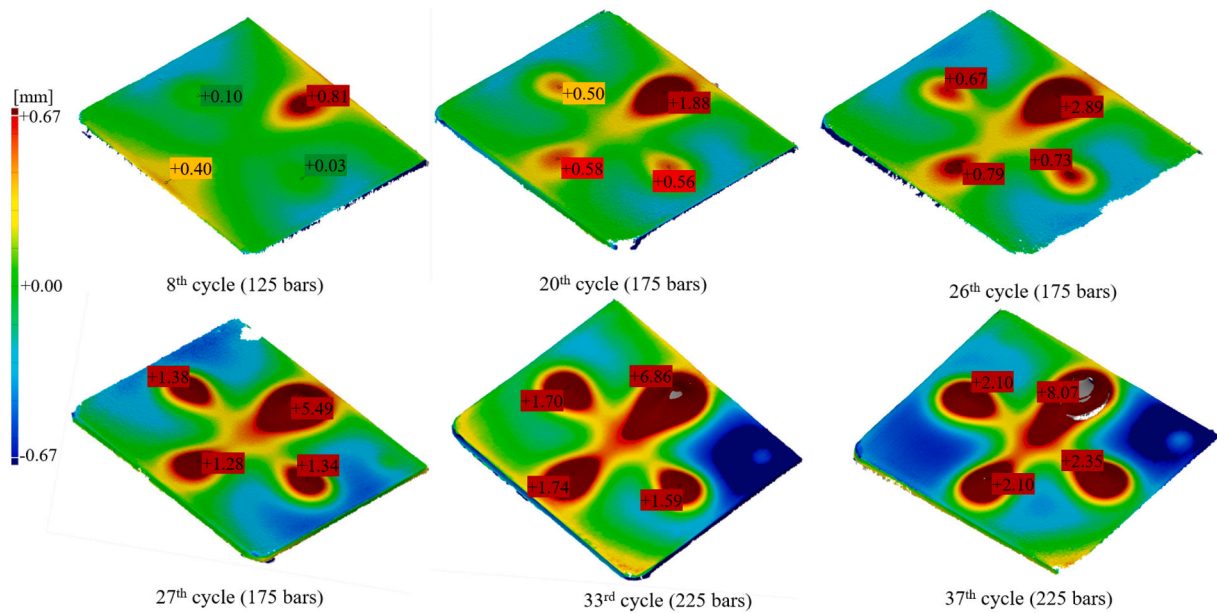
Fig. 16. 3D scanned images of the injection moulded products.

severely rose above the other slots as well. Deformation near the gate went from 2.89 mm in the 26th cycle to 5.49 mm just in the 27th cycle, which also indicates that crack initiation occurred in this interval. From this point on, a progressive failure can be seen at the near gate location as the injected melt formed an ever larger wedge that pierced the cavity surface.

3.5. Correlation between strain and cavity pressure

Correlating cavity pressure maximum and maximal relative strain at far gate location characterizes the stiffness of mould inserts because we measured cavity pressure right at the location of strain measurement. We plotted these diagrams separately for constant holding pressure and increasing holding pressure parts of the injection moulding series. Fig. 17 presents correlational diagrams for a constant holding pressure of 75 bar a), increasing holding pressure from 50 bar to 200 bar b), and constant holding pressures of 125 bars and 175 bars c). Fig. 17 a) and c) characterize the reproducibility of the process as several cycles were injection moulded at constant holding pressure. The cycles with a holding pressure of 75 bar were earlier in the injection moulding series, where the dimensional accuracy of the products was more satisfactory.

The scatter in maximal cavity pressure and maximal relative strain is also lower, ranging between 67.5 bar to 81.5 bar and 0.15 % to 0.20 %, respectively. After the 75 constant holding pressure section, we continued injection moulding and increased holding pressure from 50 bars, reaching 200 bars when the near gate strain gauge failed. This caused a gradual increase in maximal relative strain, and the slope of the measurement series corresponds to mould insert stiffness. As was shown in Fig. 13 a) and b), local thickness deviations were measured at the slot far from the gate that correspond well with the increasing maximal relative strain in Fig. 17 b). The last part of the epoxy acrylate insert strain measurement series was with a constant holding pressure of 125 and 175 bar, where the measured points show higher scatter (Fig. 17 c)) compared to when holding pressure was 75 bar. The increase in scatter is likely caused by the ever more severe deformation of the insert (shown in Fig. 14 d), and therefore the injection moulded products (shown in Fig. 16). A comparison of Fig. 17 a) and c) shows that maximal cavity pressure decreased but maximal relative strain mostly increased with higher holding pressures. Locally increasing cavity thickness necessarily increased maximal relative strain.

In the case of the aluminium insert, a positive correlation can also be observed but there is more scatter. A comparison of the maximal relative
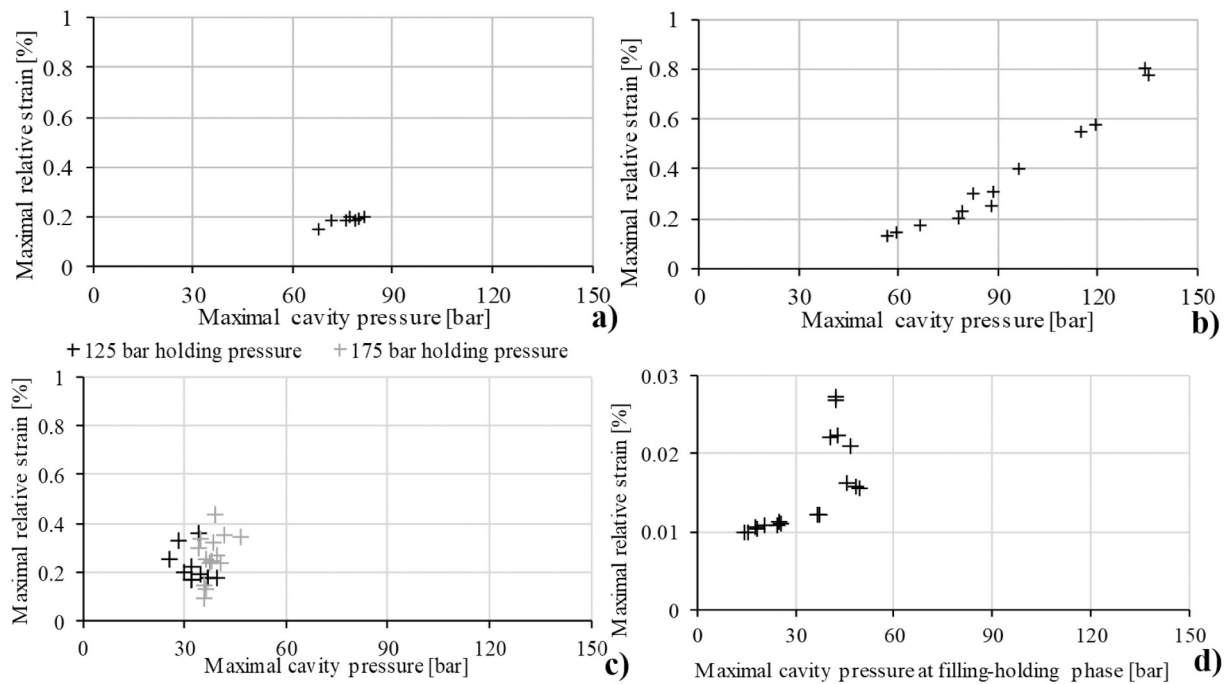
Fig. 17. Correlational diagram of the epoxy acrylate mould insert with a holding pressure of a constant 75 bar a), increasing holding pressure (from 50 bar to 200 bar) b) and with constant holding pressures of 125 and 175 bar c). Correlational diagram of the aluminium insert with increasing holding pressure (from 50 bar to 200 bar) d).

strains of the aluminium insert with the epoxy acrylate insert shows that the more than one order of magnitude difference in the moduli of elasticity of the two materials results in a large deviation of maximal relative strains.

4. Conclusion

We created a comprehensive state monitoring method where we measured operational strains, cavity pressure, surface temperature and the temperature of the back side of mould inserts. This research paper illustrates an in-depth comparison of the operational behaviour of additively manufactured (PolyJet printed) and conventional, machined aluminium prototype injection mould inserts.

During the injection moulding cycles, at near the gate and far from the gate locations, absolute strain gradually increased from cycle to cycle, even when moulding parameters were kept constant. Absolute strain (near the gate) grew from 0.22 % in the 1st cycle to 0.74 % by the end of the constant moulding parameters section. Due to the accumulation of strain (caused by the increase in the viscoelastic and the viscous deformations), we introduced relative strain to characterize the change of strain within a single cycle. We compared relative strains of epoxy acrylate and aluminium inserts when holding pressure was 75 bar and found a difference of more than an order of magnitude between the two (0.40 % of the epoxy acrylate insert, compared to the 0.017 % of the aluminium insert). Thermal camera images showed that heat conduction from the cavity surface towards the back side of the insert is very slow in the case of the epoxy acrylate material. A long delay time (~250 s) was necessary to allow the temperatures of the back side and the cavity surface to come to an equilibrium. However, the cavity surface of the aluminium insert had already cooled to ambient temperature by mould opening and the temperature of the back of the insert first rapidly increased (in the holding and residual cooling phases) and then cooled much faster in the delay time, compared to the epoxy acrylate insert.

Next, we gradually increased holding pressure from 50 bar in 25 bar steps in every second cycle. As holding pressure increased, we observed higher relative strains in the holding and residual cooling phases (1.18

% maximal relative strain at 125 bars holding pressure and 1.97 % at 175 bars, both measured near the gate). Higher holding pressure also resulted in a higher cavity pressure maximum and slower decrease. Due to the viscoelasticity of epoxy acrylate, there was a delay between the maximum of cavity pressure and the maximum of relative strain (~12 s in the presented case). This delay also increased at higher holding pressures. After injection moulding, we 3D scanned the moving side insert and two products injection moulded with high holding pressures. Scanning the mould insert did not show significant residual deformations, while scanning the product yielded noticeable deviation from the nominal product size that is caused by the elastic and viscoelastic deformations of the mould insert.

After 3D scanning, we reassembled the mould and continued injection moulding with three different holding pressures (125, 175 and 225 bar). As we increased the number of cycles, relative strain curves decreased and their shape changed. We continued increasing the load and we injection moulded until the insert failed. We identified the relative strain–time curve where a crack appeared and continued injection moulding until the mould insert failed. The injected melt pierced through the cavity wall above the near-gate slot. On the injection moulded products, we also observed ever greater shape deviations.

We set up correlational diagrams from the cavity pressure maximum and relative strain maximum results of the injection moulding series. Those corresponding to constant injection moulding parameters characterize the reproducibility of injection moulding. In this case, a small scatter of the points is desirable. On the other hand, correlational diagrams corresponding to increasing holding pressures characterize mould insert stiffness.

Our measurement system is able to quantify main operational parameters of additively manufactured mould inserts and to highlight the main differences between conventional metal and polymeric mould inserts. Epoxy-acrylate inserts are suitable for low volume mould making because of their low manufacturing cost and small manufacturing time requirement, compared to conventional metal inserts. They are especially practical for mass customization of moulded products, using almost arbitrary shaped mould inserts. This measurement can also be

applied to mould inserts manufactured by different technologies and gives data for direct comparison.

Declaration of competing interest

The authors declare that they have no known competing financial interests or personal relationships that could have appeared to influence the work reported in this paper.

References

[1] Chantzis D, Liu X, Politis DJ, Shi Z, Wang L. Design for additive manufacturing (DfAM) of hot stamping dies with improved cooling performance under cyclic loading conditions. Addit Manuf 2021;37:101720.

[2] Bai Y, Yang Y, Xiao Z, Wang D. Selective laser melting of maraging steel: mechanical properties development and its application in mold. Rapid Prototyp J 2018;24(3):623–9.

[3] Kirchheim A, Katrodiya Y, Zumofen L, Ehrig F, Wick C. Dynamic conformal cooling improves injection molding. Int J Adv Manuf Technol 2021;114:107–16.

[4] Zink B, Szabó F, Hatos I, Suplicz A, Kovács NK, Hargitai H, Tábi T, Kovács JG. Enhanced injection molding simulation of advanced injection molds. Polymers 2017;9:77.

[5] Abbès B, Abbès F, Abdessalam H, Upganlawar A. Finite element cooling simulations of conformal cooling hybrid injection molding tools manufactured by selective laser melting. Int J Adv Manuf Technol 2019;103:2515–22.

[6] Mazur M, Brincat P, Leary M, Brandt M. Numerical and experimental evaluation of a conformally cooled H13 steel injection mould manufactured with selective laser melting. Int J Adv Manuf Technol 2017;93:881–900.

[7] Samei J, Asgari H, Pelligra C, Sanjari M, Salavati S, Shahriari A, Amirmaleki M, Jahanbakht M, Hadadzadeh A, Amirkhiz BS, Mohammadi M. A hybrid additively manufactured martensitic-maraging stainless steel with superior strength and corrosion resistance for plastic injection molding dies. Addit Manuf 2021;45:102068.

[8] Nagahanumaiah B. Ravi: effects of injection molding parameters on shrinkage and weight of plastic part produced by DMLS mold. Rapid Prototyp J 2009;15(3):179–86.

[9] Ilyas I, Taylor C, Dalgarno K, Gosden J. Design and manufacture of injection mould tool inserts produced using indirect SLS and machining processes. Rapid Prototyp J 2010;16(6):429–40.

[10] Masood SH. W.Q song: development of new metal/polymer materials for rapid tooling using fused deposition modelling. Mater Des 2004;25(7):587–94.

[11] Huang MZ, Schlarb AK. The effect of different processing, injection molding (IM) and fused deposition modeling (FDM), on the environmental stress cracking (ESC) behavior of filled and unfilled polycarbonate (PC). eXPRESSPolymer Letters 2021;15:194–202.

[12] Boros R, Kannan Rajamani P, Kovács JG. Combination of 3D printing and injection molding: overmolding and overprinting eXPRESS polymer. Letters 2019;13:889–97.

[13] Hanon MM, Marczis R, Zsidai L. Influence of the 3D printing process settings on tensile strength of PLA and HT-PLA. Period Polytechn Mech Eng 2021;65(1):38–46.

[14] Gohn AM, Brown D, Mendis G, Forster S, Rudd N, Giles M. Mold inserts for injection molding prototype applications fabricated via material extrusion additive manufacturing. Addit Manuf 2022;51:102595.

[15] Farioli D, Strano M, Vangosa FB, Zaragoza VG, Aicardi A. Rapid tooling for injection molding inserts. In: ESAFORM 2021; 2021.

[16] Sehhat MH, Mahdianikhotbesara A, Yadegari F. Impact of temperature and material variation on mechanical properties of parts fabricated with fused deposition modeling (FDM) additive manufacturing. Int J Adv Manuf Technol 2022;120:4791–801.

[17] Hassanifard S, Behdinan K. Effects of voids and raster orientations on fatigue life of notched additively manufactured PLA components. Int J Adv Manuf Technol 2022;120:6241–50.

[18] Bernal JDBerrio, Silva ECN, Rubio WMontealegre. Characterization of effective Young's modulus for fused deposition modeling manufactured topology optimization designs. The International Journal of Advanced Manufacturing Technology 2019;103:2879–92.

[19] Vahed R, Zareie Rajani HR, Milani AS. Can a black-box AI replace costly DMA Testing?—A case study on prediction and optimization of dynamic mechanical properties of 3D printed acrylonitrile butadiene styrene. Materials 2022;15:2855.

[20] Zhu Q, Yu K, Li H, et al. Rapid residual stress prediction and feedback control during fused deposition modeling of PLA. Int J Adv Manuf Technol 2022;118:3229–40.

[21] Kuo CC, Wu YR, Li MH, et al. Minimizing warpage of ABS prototypes built with low-cost fused deposition modeling machine using developed closed-chamber and optimal process parameters. Int J Adv Manuf Technol 2019;101:593–602.

[22] Ding H, Zeng C, Raush J, Momeni K, Guo S. Developing fused deposition modeling additive manufacturing processing strategies for aluminum alloy 7075: sample preparation and metallographic characterization. Materials 2022;15:1340.

[23] Minetola P, Calignano F, Galati M. Comparing geometric tolerance capabilities of additive manufacturing systems for polymers. Addit Manuf 2020;32:101103.

[24] Kuo C-C, Qiu S-X, Lee G-Y, Zhou J, He H-Q. Characterizations of polymer injection molding tools with conformal cooling channels fabricated by direct and indirect rapid tooling technologies. Int J Adv Manuf Technol 2021;117:343–60.

[25] Choe C-M, Yang W-C, Kim U-H, Ri B-G, Om M-S. Manufacture of centrifugal compressor impeller using FDM and investment casting. Int J Adv Manuf Technol 2022;118:173–81.

[26] Taylor HL, Bheemreddy V, Iyibilgin O, Leu M, Chandrashekhara K. Modeling and characterization of fused deposition modeling tooling for vacuum assisted resin transfer molding process. Addit Manuf 2015;7:64–72.

[27] Sz G, Krizsma NK, Kovács JG, Kovács A. Suplicz: in-situ monitoring of deformation in rapid prototyped injection molds. Addit Manuf 2021;42. 102001/1–102001/8.

[28] Zink B, Kovács NK, Kovács JG. Thermal analysis based method development for novel rapid tooling applications. Int Commun Heat Mass Transf 2019;108:104297.

[29] Zink B, Kovács JG. Enhancing thermal simulations for prototype molds. Period Polytechn Mech Eng 2018;62(4):320–5.

[30] Davoudinejad A, Bayat M, Pedersen DB, Zhang Y, Hattel JH, Tosello G. Experimental investigation and thermo-mechanical modelling for tool life evaluation of photopolymer additively manufactured mould inserts in different injection moulding conditions. Int J Adv Manuf Technol 2019;102:403–20.

[31] Dizon JRC, Valino AD, Souza LR, Espera Jr AH, Chen Q, Advincula RC. Three-dimensional-printed molds and materials for injection molding and rapid tooling applications. MRS Communications 2019;9:1267–83.

[32] Wang D, Dong A, Zhu G, Shu D, Sun J, Li F, Sun B. Rapid casting of complex impeller based on 3D printing wax pattern and simulation optimization. Int J Adv Manuf Technol 2019;100:2629–35.

[33] Wick-Joliat R, Tschamper M, Kontic R, Penner D. Water-soluble sacrificial 3D printed molds for fast prototyping in ceramic injection molding. Addit Manuf 2021;48:102408.

[34] Mendible GA, Saleh N, Barry C, Johnston SP. Mechanical properties and crystallinity of polypropylene injection molded in polyjet and aluminum tooling. Rapid Prototyp J 2022;28(4):686–94.

[35] Tábi T, Kovács NK, Sajó IE, Czigány T, Hajba S, Kovács JG. Comparison of thermal, mechanical and thermomechanical properties of poly(lactic acid) injection-molded into epoxy-based rapid prototyped (PolyJet) and conventional steel mold. J Therm Anal Calorimetry 2016;123:349–61.

[36] Bagalkot A, Pons D, Clucas D, Symons D. A methodology for setting the injection moulding process parameters for polymer rapid tooling inserts. Rapid Prototyp J 2019;25(9):1493–505.

[37] Kovács JG, Szabó F, Kovács NK, Suplicz A, Zink B, Tábi T, Hargitai H. Thermal simulations and measurements for rapid tool inserts in injection molding applications. Appl Therm Eng 2015;85(25):44–51.